





Photon statistics of organic polariton condensates

Anton D. Putintsev ^{1,*} Anton V. Zasedatelev,¹ Vladislav Yu. Shishkov,^{1,2,3} Mikhail Misko ¹ Denis A. Sannikov,¹ Evgeny S. Andrianov,^{1,2,3} Yurii E. Lozovik,^{1,2,4,5,†} Ullrich Scherf ⁶ and Pavlos G. Lagoudakis ¹

¹Hybrid Photonics Laboratory, Skolkovo Institute of Science and Technology, Territory of Innovation Center Skolkovo, Bolshoy Boulevard 30, Building 1, 121205 Moscow, Russia

²Dukhov Research Institute of Automatics (VNIIA), 127055 Moscow, Russia

³Moscow Institute of Physics and Technology, 141701 Dolgoprudny, Russia

⁴Institute for Spectroscopy, RAS, 108840 Troitsk, Russia

⁵Moscow Institute of Electronics and Mathematics, National Research University Higher School of Economics, 123592 Moscow, Russia

⁶Macromolecular Chemistry Group and Institute for Polymer Technology, Bergische Universität Wuppertal, 42119 Wuppertal, Germany



(Received 9 April 2024; revised 21 June 2024; accepted 24 June 2024; published 15 July 2024)

We report on the quantum statistical properties of organic polariton condensates. Our experimental study demonstrates low particle number fluctuations for highly populated condensates at room temperature. We show a quantum noise of the condensate that is ~ 100 times the shot-noise limit of an ideal coherent light source, setting the lower limit of the noise for organic polariton devices. Despite the high thermal fluctuations at room temperature, strong dynamical instability, and static disorder intrinsic to organic systems, the condensate exhibits an extremely high degree of second-order coherence $g^{(2)}(\tau = 0)$ down to $1.00034 \pm 1 \times 10^{-5}$. We elucidate a nontrivial behavior in the second-order coherence of the condensate with its spatial extension. Unlike a conventional laser, the organic polariton condensate tends to increase its noise level above shot-noise fluctuations due to a complex interplay between polariton thermalization, cavity lifetime, and kinetic losses originating from the quantum fluid properties of polariton condensates.

DOI: [10.1103/PhysRevB.110.045125](https://doi.org/10.1103/PhysRevB.110.045125)

I. INTRODUCTION

Macroscopic quantum phenomena in exciton-polariton (hereinafter polariton) systems are the subject of extensive research going far beyond purely fundamental interest [1–4]. Advances in semiconductor technology and material science within the last decade have led to several new promising platforms [5–15] enabling room temperature operation. Organic microcavities are the ones that have been flourishing, demonstrating spontaneously formed [16] and seeded [1] coherent polariton phases, Bose-Einstein condensation [17], superfluidity [18], and features of many-body interactions in condensate lattices [7,19] at room temperature. Much attention has been paid to understanding the coherent nature of organic polariton condensates and its relation to on-site nonlinearities [6,20] as well as disorder [21,22]. Long-range order and temporal coherence of polariton condensates at room temperature have been shown by means of Michelson interferometry and via line narrowing in spectroscopic measurements [6,17,23–25]. Although first-order coherence is essential to manifest Bose-Einstein condensate (BEC) formation, in principle, it cannot discriminate between coherent and thermal states due to the lack of quantum statistical information about light.

The quantum statistics of weakly interacting BECs of ultracold atoms resembles a Poissonian distribution like an

ideal laser [26]. In this respect polariton BECs can be very different from atomic ones [27,28]. High thermal fluctuations [29], on-site nonlinearities [30–32], and condensate depletion [33,34] as well as mode competition [35] can significantly broaden the particle number distribution, thereby increasing quantum fluctuations way above the shot-noise limit. The quantum statistics of solid-state BECs, besides their fundamental importance, have a certain connection to applications. In a way similar to how laser shot noise defines limits for laser cooling [36] and precise interferometry [37], noise in polariton condensates sets boundaries for emerging polariton applications [1,35,38–46]. In a recent report on single-photon switching, Zasedatelev *et al.* [47] highlighted the role of shot-to-shot intensity fluctuations of the condensate that compromise switching fidelity. Thus, understanding the quantum statistics is crucial in view of novel devices.

Until now, second-order coherence and the photon statistics of room temperature polariton condensates have remained unexplored territory. From a theoretical point of view, polariton BECs are complex open dissipative systems which intrinsically are far from equilibrium [48]. Moreover, unlike polariton BECs in a cryogenic environment, room temperature systems are also subject to high thermal fluctuations and strong spatial disorder inherent in most practical structures [21], rendering them extremely challenging for a theoretical study. On the experimental side, the main problem is the subpicosecond polariton dynamics that cannot be acquired in standard Hanbury-Brown and Twiss measurements due to the insufficient time resolution of single-photon avalanche photodetectors of ~ 40 ps [49]. Advanced techniques for high-

*Contact author: anton.putintsev@skoltech.ru

†Deceased.

order correlation measurements based on photon counting with a streak camera [50,51] enable more than an order of magnitude improvement in time resolution but are still limited to a few picoseconds [52] and, usually, in the case of inorganic microcavities, require high repetition rates of $\sim 10^8$ Hz to collect enough photon statistics. Even though organic polariton emission is more intense and the repetition rate can be lowered, intrinsic photobleaching of organic microcavities does not allow them to tolerate more than roughly several million pulses [47,53].

In this work we develop an alternative approach to access second-order coherence based on well-controlled single-shot detection allowing for direct measurements of photon statistics of polariton condensates. Similar approaches relying on single photodetector measurements have been used previously to study second-order coherence in atomic condensates [26,54]. Using this technique, we demonstrate an unexpectedly low excessive quantum noise of around 1.9% for spatially highly fragmented organic polariton BECs at room temperature. Reducing the size of the system increases the condensation threshold, nonlinearities, and effective polariton thermalization rate due to kinetic losses originating from ballistic propagation of polaritons out of the condensate area. However, it does not reduce the degree of fragmentation in a condensate, which was discussed in recent reports [22,55], and instead enhances shot-to-shot fluctuations.

II. PHOTON STATISTICS OF A CONDENSATE

Here we utilize methyl-substituted ladder-type poly(paraphenylene) (MeLPPP) to realize polariton physics [1,17,47,56]. The cavity design consists of a thin 35 nm film of MeLPPP placed between two 50 nm spacers of SiO₂, which in turn are sandwiched between two SiO₂/Ta₂O₅ distributed Bragg reflectors on a glass substrate. This $\lambda/2$ organic microcavity exhibits an energy splitting of $\Omega = 150$ meV (Rabi splitting) between the exciton resonance (2.72 eV) and the lower polariton branch (LPB; 2.582 eV), which is of the order of detuning between the bare cavity and the exciton modes, fixed across all sets of measurements in this work ($\delta = 140$ meV). In particular, Hopfield coefficients, or exciton and cavity photon fractions, for the lower polariton state are $|X|^2 = [1 + \delta/\sqrt{(\delta^2 + \Omega^2)}]/2 = 0.162$ and $|C|^2 = [1 - \delta/\sqrt{(\delta^2 + \Omega^2)}]/2 = 0.838$, respectively.

We employ nonresonant 2 ps pulsed excitation at 400 nm and a 10 Hz repetition rate focused down to a 44 μm spot size and measure 300 successive single exciton-polariton realizations. To exclude laboratory noise and laser drifts we postselect only those realizations that correspond to the $\pm 1\%$ range of the input pump pulse energy. As a result, we observe fluctuations of the total polariton population in a condensate of up to 10% from the average value from realization to realization at a fixed excitation fluence [$\pm 1\%$; see Fig. 1(a)]. Increasing the pump fluence leads to an increase in the average polariton population in a condensate according to the pump-power dependence [Fig. 1(b), right axis] and simultaneously to the narrowing of the polariton population distribution, as shown by the different colors in Fig. 1(a).

To quantify shot noise in the system we introduce the Fano factor, $F = \sigma_{\bar{n}}^2/\bar{n}$, which shows the deviation from pure

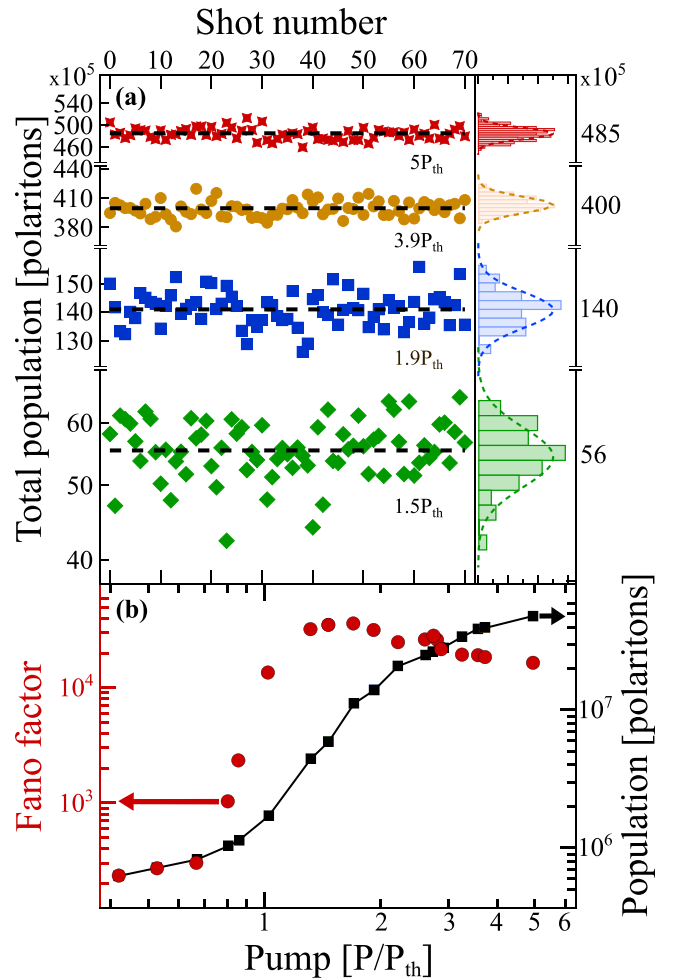


FIG. 1. (a) Fluctuations of the total polariton number in a condensate at four different excitation pump fluences: $1.5P_{\text{th}}$, $1.9P_{\text{th}}$, $3.9P_{\text{th}}$, and $5P_{\text{th}}$, plotted with green, blue, orange, and red markers, respectively, for a spot size with a FWHM of 44 μm . The right panel shows corresponding histograms of shot-to-shot particle number fluctuations (photon statistics). (b) Dependence of the Fano factor (red) and average polariton population (black) on excitation fluency. Red and black arrows point to the relevant axis.

Poissonian statistics (with $F = 1$). Figure 1(b) (left axis) demonstrates a rapid increase in noise in our system near the condensation threshold, followed by a slight decrease. Both the broadening of the Fano factor and its deviation from a pure coherent state originate from the non-steady-state nature and losses of the condensate as well as finite-size effects [57]. The time-averaged zero-time-delay second-order particle correlation function is given by

$$\overline{g^{(2)}(0)} = 1 + \frac{\sigma_{\bar{n}}^2 - \bar{n}}{\bar{n}^2}, \quad (1)$$

where \bar{n} is the ensemble-averaged number of polaritons in a condensate, or total population, and $\sigma_{\bar{n}}^2$ is the variance of this number. Time averaging results from the fact that even though we deal with pulse-driven polariton condensates and operate in a single-shot detection regime, we still integrate all the emission over the condensate duration, which is strongly dependent on the excitation duration time. For the current

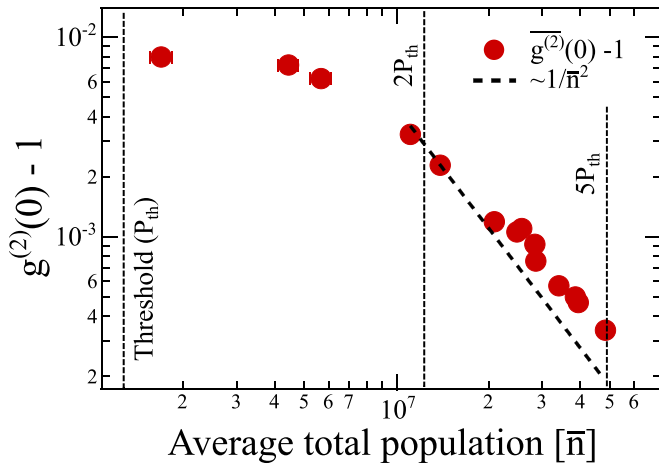


FIG. 2. Zero-time-delay second-order correlation function of the polariton condensate as a function of total polariton population. Red dots represent measured $\langle g_s^{(2)}(0) - 1 \rangle$ time-averaged values calculated from experimental data shown in Fig. 1(b). Vertical black dashed lines indicate the average total polariton population at the condensation threshold, 2 times the condensation threshold, and 5 times the condensation threshold, from left to right. The nonvertical black dashed line represents a fit of the experimental data with an $\sim 1/\bar{n}^2$ function.

pumping conditions with 2 ps pump pulses we measure the autocorrelation function of the polariton condensate emission and derive the lifetime of a single condensate realization to be ~ 2.8 ps. This result is supported by our recently developed microscopic model (for details see Sec. 1 in the Supplemental Material (SM) [58]). Moreover, the value of the average second-order coherence depends on the relation between the time resolution in our experiment and the intensity correlation time as a factor of $\sim \frac{\tau_c}{(\Delta T + \tau_c)}$ [59]. In Sec. 1 of the SM [58] we discuss the above relation and conclude that the condensation lifetime limits the coherence in the system, while the second-order coherence function, which is integrated over the condensate lifetime, provides actual values of $g^{(2)}(\tau = 0)$ in the region above $\approx 2P_{th}$. This renders this approach to measure zero-time-delay second-order coherence a powerful tool to probe photon statistics of polariton condensates at room temperature. It is noteworthy that we do not immediately observe values of $g^{(2)}(0) = 2$ anywhere in the vicinity of or below the polariton condensation threshold due to the insufficient time resolution with respect to the intensity correlation time and the multimode nature of the system emission in this region of pumping powers, which skews the observed results. However, we demonstrate thermal statistics with $g^{(2)}(0) \geq 1.5$ below the condensation threshold by taking into account mode composition, time resolution, and the dark noise of the detection (for details see Sec. 1 in the SM [58]).

Since for coherent light-matter waves $g^{(2)}(0) = 1$ and for strongly fluctuating condensates $g^{(2)}(0) > 1$, we observe a rapid transition of the system from an incoherent to a coherent state, as we do the power scan from $0.4P_{th}$ to $5P_{th}$. Figure 2 shows above-threshold values (for the full scan see Sec. 1 in the SM [58]), reaching a quite noiseless, second-order coherent condensation regime with the lowest measured value being $g^{(2)}(0) = 1.00034 \pm 1 \times 10^{-5}$ at $5P_{th}$,

implying that the intrinsic particle number fluctuation of a coherent state is around 100 times above the shot-noise limit. This result is rather surprising considering the large dynamical instability and disorder inherent in organic systems when studied in the single-shot excitation regime. Such a low-noise regime is reached at gain saturation, as one can see from the pump-power intensity dependence of the photoluminescence emission in Fig. 1(b) (right axis). Accounting for the fact that we are dealing with $\sim 10^7$ polaritons in the system, we can neglect the term $1/\bar{n}$ in Eq. (1), and hence, Fig. 2 essentially shows the dependence of σ_n^2/\bar{n}^2 on \bar{n} . Since we observe good agreement with the fit function $\sim 1/\bar{n}^2$, we can conclude that σ_n^2 is a weakly growing function of an average total polariton population \bar{n} , while in the classical case the laboratory noise is defined by fluctuations of an average photon number n and $\sigma^2 \sim n^2$ [60]. Therefore, from Fig. 2 we can infer that the noise in our system manifests the thermal and quantum nature of BECs that can be witnessed by the widths of the photon number distributions depicted in Fig. 1(a).

III. ROLE OF KINETIC LOSSES AND DISORDER

Instability and disorder were the subject of recent works in which the origins of spatial filamentation, or fragmentation, of polariton condensates [21,22,55] were experimentally studied. Condensate filamentation under single-shot excitation in high- Q GaAs-based microcavities was attributed to effective self-focusing, or hole burning, which caused the appearance of a prevailing contribution of the effective attractive interaction over the repulsive mean-field one for highly photonic polaritons [55]. This effect is possible in the regime of short-pulse excitation, allowing for complete depletion of the exciton reservoir within a single realization of the condensate; however, it is unlikely to be the case in our system, as we deal with 2 ps pulsed excitation and an ≈ 280 fs polariton lifetime that, once above the condensation threshold, works as a quasistationary excitation that continuously replenishes and effectively clamps the exciton reservoir under stimulated depletion towards the condensate. For organic systems, the role of disorder in condensate fragmentation was first discussed by Daskalakis *et al.* [21]. Work by Bobrovska *et al.* [22] experimentally demonstrated the dynamical instability of condensates leading to the formation of multiple spatial domains and depending on the size of spatial pump profiles. Moreover, the authors experimentally demonstrated mutual coherence between fragments in the highly disordered condensate, as well as long-range spatial coherence.

To reduce the degree of fragmentation, we vary the pump size of the Gaussian beam in the range between 9 and 44 μm . Figures 3(a) and 3(b) show real-space images of single condensate realizations formed by 44 and 14 μm pump spots, respectively. Corresponding k -space images obtained under the same pumping conditions are presented in Figs. 3(c) and 3(d). The experiment shows that instability is equally present regardless of the size of the condensates. Importantly, we observe a broadening of the polariton distribution in the momentum space by decreasing the spot size [Figs. 3(e) and 3(f)], evidencing an increase in the average group velocity of polaritons, i.e., the tendency to occupy higher-momentum

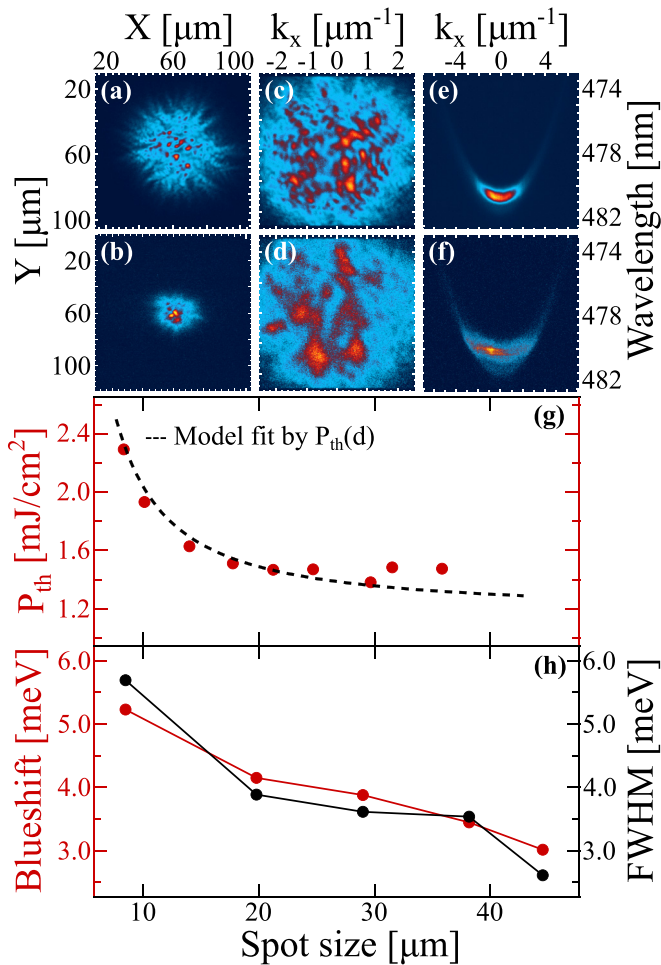


FIG. 3. (a) and (b) Real-space images of single condensate realizations obtained at two thresholds for two different excitation spot sizes: 44 and 14 μm at FWHM, respectively. (c) and (d) Corresponding single-shot images in momentum space obtained with the same excitation conditions and (e) and (f) dispersion images integrated over 500 single-shot realizations. Color scales of all images are normalized to their maxima. (g) Condensation threshold as a function of excitation spot size. (h) Blueshift and linewidth at FWHM of the condensate as a function of excitation spot size. The data were obtained by averaging over 40 E, k distributions of single condensate realizations for each spot size.

states because more kinetic energy outflows from the condensation area within its lifetime.

The expansion in momentum space is accompanied by an increase in the condensation threshold for small spot sizes. This leads to the hypothesis that kinetic losses of polaritons from the condensate due to polariton outflow are larger for smaller sizes, and hence, with larger losses a higher density of excitons is needed to reach the threshold. We consider the threshold pump fluence P_{th} to be proportional to the total losses γ from the LPB:

$$P_{\text{th}} \propto \gamma. \quad (2)$$

There are two major channels in the energy dissipation rate of polaritons: the internal radiative losses that correspond to the photon leakage from the cavity γ_0 and the external losses that occur due to the outflow of polaritons from the pumped

area γ_{out} , which can be estimated as follows:

$$\gamma_{\text{out}} = \frac{\langle v_{\text{gr}} \rangle L}{S}, \quad (3)$$

where $\langle v_{\text{gr}} \rangle$ is the average group velocity of the polaritons leaking from the pumped spot, L is the circumference of the pumped area, and S is the area of the spot. Assuming that the excited area is a circle of diameter d and $\gamma = \gamma_0 + \gamma_{\text{out}}$, we obtain the following dependence for the threshold excitation fluence:

$$P_{\text{th}}(d) = P_{\text{th}}(\infty) \left(1 + \frac{4\langle v_{\text{gr}} \rangle}{\gamma_0 d} \right), \quad (4)$$

where $P_{\text{th}}(\infty)$ is the threshold pump fluence in the limit of large spot size ($d \gg \gamma_0 / \langle v_{\text{gr}} \rangle$).

From dispersion imaging below threshold we extract internal radiative losses $\gamma_0 = 3.7 \times 10^{-3}$ [eV]. From dispersion images above threshold we extract the dependence of the average group velocity of polaritons on the excitation spot size $\langle v_{\text{gr}} \rangle(d)$ (for details see Sec. 2 in the SM [58]), which increases with decreasing spot size. Using formula (4), we fit the experimentally obtained threshold incident fluence values [Fig. 3(g), red axis] and obtain the best fit result: $P_{\text{th}}(\infty) \approx 1.2$ mJ/cm². The experiment shows that the condensation threshold reaches a plateau of $P_{\text{th}}^{\text{exp}}(\infty) \approx 1.5$ mJ/cm² above a certain spot size. We observe a quantitative agreement within $\approx 25\%$ deviation from the best fit result of a threshold constant. One should keep in mind that the present model is linear; i.e., it does not include nonlinear effects (for instance, blueshift) [6,20,23].

Moreover, the nonlinear threshold behavior is accompanied by a significant increase in the condensate blueshift with decreasing excitation spot size. Fixing the pump fluence at around $2P_{\text{th}}$, we record a single-shot dispersion image for five different spot sizes. Averaging dispersion images over 40 realizations at each spot size, we observe an increasing blueshift with decreasing spot size [Fig. 3(h), red axis]. This effect is accompanied by a broadening of the condensate linewidth of the spectra integrated over $\pm 5 \mu\text{m}^{-1}$ [Fig. 3(h), black axis]. The buildup of coherence in a condensate is affected by many parameters of the system, such as intrinsic nonlinearity [61], the lifetime of the exciton reservoir [62], the presence of dark excitons [63], and characteristic times of relaxation processes [64]. In our experiment the temporal coherence is rather limited by the dynamical blueshift that smears out the linewidth within the pump pulse duration and the condensate lifetime.

IV. FINITE-SIZE EFFECTS

In this section, we investigate the influence of the system size on the statistics of the polariton emission. To explore the behavior of quantum noise in the condensate, we vary the pump size of the Gaussian beam in the range between 14 and 59 μm and extract the $g^{(2)}(0)$ values for seven different spot sizes under the same pumping conditions. To exclude any bias from sample inhomogeneity, each spot size value aggregates eight different positions on the sample with 300 successive realizations collected. To minimize fluctuations of the condensate occupancy due to pump-induced exciton reservoir density variations and to avoid photodegradation at small spot sizes, we fix the excitation pump fluence at $2P_{\text{th}} \pm 1\%$. We

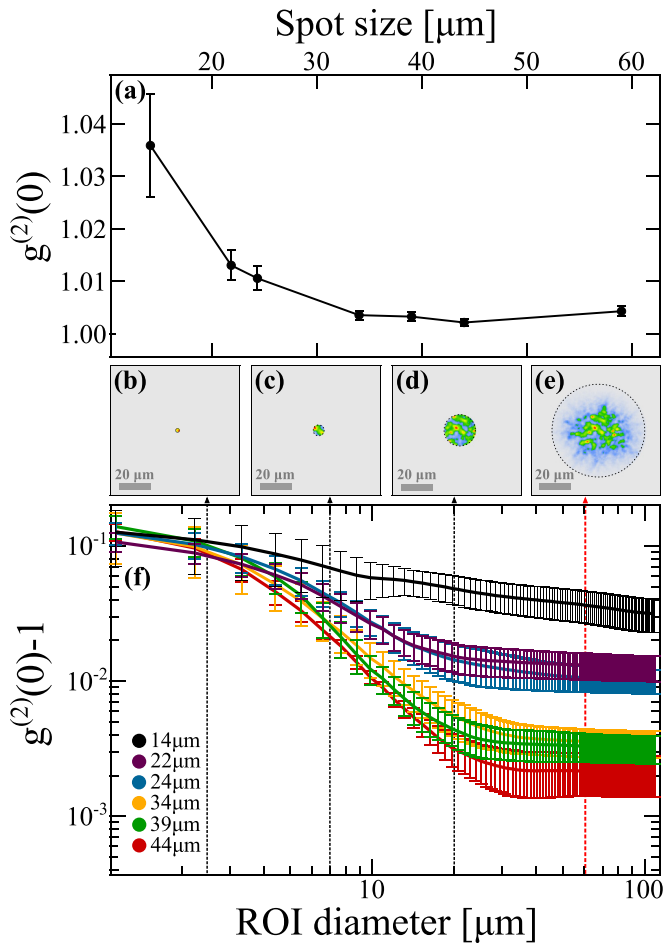


FIG. 4. (a) The second-order coherence function at zero time delay at $\sim 2P_{\text{th}}$ as a function of an excitation spot size corresponding to cross-section values along the red dashed line in (f). (b)–(e) Plots visualizing region of interest (ROI) masks applied to the real-space profile of a 44 μm condensate. Color scales are normalized to the maxima of the images. (f) Dependence of the calculated $g^{(2)}(0) - 1$ values on the ROI size within which the real-space polariton intensity is integrated for different spot sizes of the condensate: 14, 22, 24, 34, 39, and 44 μm . Each point of each curve is averaged over eight different positions on the sample, and error bars represent the spread.

observe substantial growth in the shot noise of the condensate upon decreasing the size of the pumping spot, as shown in Fig. 4(a). To make sure that this effect has a physical nature rather than being an artifact of analysis or measured instrumental noises, we examine how the calculated $g^{(2)}(0)$ values depend on the region of interest (ROI) of an integrated area of single-shot images for all available sets of condensate images for different spot sizes. We apply a circular mask with the diameter varying from 1 to 100 μm to real-space images of single condensate realizations [Figs. 4(b)–4(e)] and calculate $g^{(2)}(0)$ values for each of the mask diameters [Fig. 4(f)]. We observe that upon increasing the diameter of the mask in real space, the contribution of stochastic disorder to $g^{(2)}(0)$ decreases. From $\approx 30 \mu\text{m}$ ROI diameter, condensates of all sizes reach their plateaus. We observe that with increasing condensate size the plateau value of the second-order coherence function at zero time delay decreases. The decline of the black

curve in Fig. 4(f) (for the condensate of the smallest size) is attributed to the increased contribution of the camera noise to the integral intensity of the image, which is reduced upon increasing the diameter of the mask. This behavior is absent in larger condensates. It is worth mentioning that prior to the analysis of the second-order coherence function we postselected only those realizations that corresponded to the $\pm 1\%$ range of the input pump pulse energy. Changing this tolerance interval from $\pm 1\%$ to $\pm 2\%$, $\pm 5\%$, or $\pm 10\%$ does not qualitatively affect the noise properties of the system and does not change the dependence observed in Fig. 4(a) (for details see Sec. 3 in the SM [58]). This implies that the intrinsic noise, originating from the process of polariton condensation rather than classical fluctuations and all laboratory-related noise, makes a major contribution to the observed statistics.

To understand the change in photon statistics with decreasing size of the condensate [Fig. 4(a)] we need a detailed picture of the mechanisms behind polariton condensation at room temperature. Therefore, we explore its behavior by reconstructing the experimental S curves [pump-power dependences; Fig. 5(a)] of polariton emission with a recently developed multimode microscopic model [47] describing the full dynamics of the system (for details see Sec. 4 in the SM). One of the dominant relaxation processes within the lower polariton branch is the thermalization mechanism [17,47], which was utilized to explain effective stimulated relaxation of polaritons towards the ground polariton state [48]. The thermalization term in the rate equations is $V_{\text{therm}}^{\text{eff}} \sim n_i(n_0 + 1)\gamma_{\text{therm}}^{\omega_i, \omega_0}$, where n_i and n_0 are polariton densities at the i th and zero (ground) energy states and $\gamma_{\text{therm}}^{\omega_i, \omega_0}$ is a thermalization rate from higher energetic polariton states $\hbar\omega_i$ towards the ground state $\hbar\omega_0$ [47]. This term evolves throughout the lifetime of the polariton system, demonstrating nontrivial dynamics. The increase in total losses at the LPB with decreasing pumping spot size leads to higher condensation thresholds, as shown in Fig. 5(a). The inset of Fig. 5(a) shows the polariton population density at the threshold, calculated from the integrated polariton emission at the threshold over the corresponding FWHM of the pumping area. Therefore, the density dependence of the thermalization term results in its increase with decreasing pumping area. However, for pumping fluences above the condensation threshold, the total losses within the LPB of smaller condensates result in smaller polariton condensate densities and therefore a reduced thermalization term (for details see Sec. 5 in the SM [58]). Overall, the size dependence of the thermalization term leads to an extension of the transition region at the crossover from a thermal to a coherent polariton state, which is evidenced by a flattening of the S curves with decreasing excitation spot size. Figure 5(b) shows the slope coefficient of the nonlinear regions for both experimental and modeled S curves, normalized to the largest slope coefficient, vs the pumping spot size. Thus, our numerical simulations qualitatively reproduce the experimental data from Fig. 5(a). This is a significant revelation that distinguishes between polariton condensation and conventional lasing in weakly coupled systems, as the increase in photon losses in conventional lasers does not change the shape of the S curves [57] but shifts them along the pumping axis, thereby increasing the lasing threshold. However, as we observe here, in polariton condensates the threshold and the shape of the S curve change

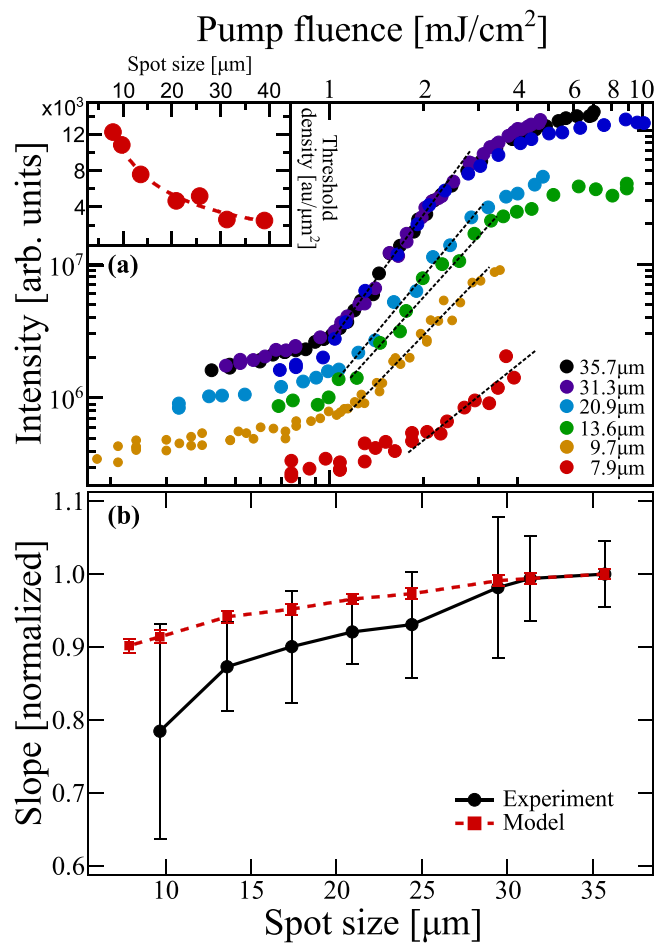


FIG. 5. Dependences of the polariton photoluminescence on pump fluence for six different dimensions of a Gaussian pump profile with FWHM values from 7.9 to 35.7 μm . (a) Experimentally obtained S curves for six different spot sizes. The inset shows the dependence of the polariton density at the condensation threshold on spot size; the red dashed line is a guide to the eye. (b) Dependences of the normalized slope coefficients of a nonlinear region of the experimental S curves on different spot sizes (black solid line) and the normalized slope coefficients of a nonlinear region of the modeled S curves on different spot sizes (red dashed line) which correspond to nine different values of polariton losses, $\gamma_{\text{out}} = \gamma_0 + \frac{(v_{\text{gr}})L}{S}$.

with increasing lateral losses, which explains the behavior of $g^{(2)}(0)$ with the change in the pump spot dimensions shown in Fig. 3(g). Being below the gain saturation regime, the condensate experiences larger excessive noise due to contributions from spontaneous relaxation, as the stimulation is undersaturated for smaller spot sizes.

Polariton interactions in the condensate, as well as interactions with the exciton reservoir, can significantly affect photon statistics by driving it from the shot-noise limit towards super-Poisson and even beyond thermal noise distributions [35]. In contrast to conventional III-V semiconductor microcavities, excitons in organic systems are highly localized (so-called Frenkel-type excitons); thus, polariton nonlinearities originating from Coulomb-exchange exciton interactions are strongly suppressed in organic polariton condensates. Nevertheless, such condensates could still be

subject to significant nonlinear blueshift, which is attributed to different mechanisms, i.e., Rabi-splitting quenching and cavity mode renormalization via weakly coupled molecules, as shown in a recent study [20]. These effects give rise to effective nonlinear interactions in organic polariton condensates, as discussed in a recent detailed study of the first-order coherence [6]. The blueshift could influence the phase coherence of the system and therefore could potentially shape the quantum noise properties of polariton condensates, which considered in the study by Love *et al.* [49]. In particular, the blueshift of the condensate does not contribute significantly to the quantum noise, as evidenced by the gradual decrease in the second-order coherence with increasing polariton population, unlike the blueshift behavior.

V. DISORDER ANALYSIS

It is important for our analysis to investigate changes in static and stochastic disorders upon changing the system size. We call the stochastic fluctuation of a real-space profile from shot to shot “stochastic disorder,” while we call fragmentation of a time-averaged real-space profile pinned by structure imperfections “static disorder.”

We analyze sets consisting of 300 measured successive single exciton-polariton realizations each for a range of different spot sizes and different positions on the sample [Figs. 6(b)–6(e)]. To exclude laboratory noise and laser drifts we postselect only those realizations that correspond to the $\pm 1\%$ range of the input pump pulse energy ($2.1P_{\text{th}}$). First, we average the resulting set of images (300 single-shot profiles) to obtain a one-position time-averaged real-space profile for a given position on the sample and given spot size [Figs. 6(f)–6(i)]. Then, we obtain a many-position time-averaged real-space profile from eight different positions on the sample for a given spot size [Figs. 6(j)–6(m)]. By conducting a pixel-to-pixel subtraction of a one-position time-averaged profile from a many-position time-averaged profile, we find the ratio between the integral of the absolute value of the subtraction and the integral of a many-position time-averaged profile. This value allows us to quantitatively assess the deviation of a time-averaged real-space profile of a condensate from a profile that tends to have an ideal two-dimensional Gaussian form (for a large number of position averages), also known as the figure of merit for static disorder. Then, we apply this method to seven different spot sizes of the system, which allows us to obtain the dependence of a static disorder on the spot size of the system, such that each blue point in Fig. 6(a) is an average of eight different positions on the sample.

Second, we characterize the stochastic disorder. We subtract a single-shot real-space profile [Figs. 6(b)–6(e)] from a one-position time-averaged one and find the ratio between the integral of the result and the integral of a one-position time-averaged profile. Excluding the contribution of the static disorder, which is position dependent and mainly arises from the active material disorder, to the stochastic disorder by applying this approach, we extract the quantitative value of such a nonlinear formation of a unique density pattern from shot to shot on top of the time-averaged landscape. In the same manner we vary the position on the sample for each red point

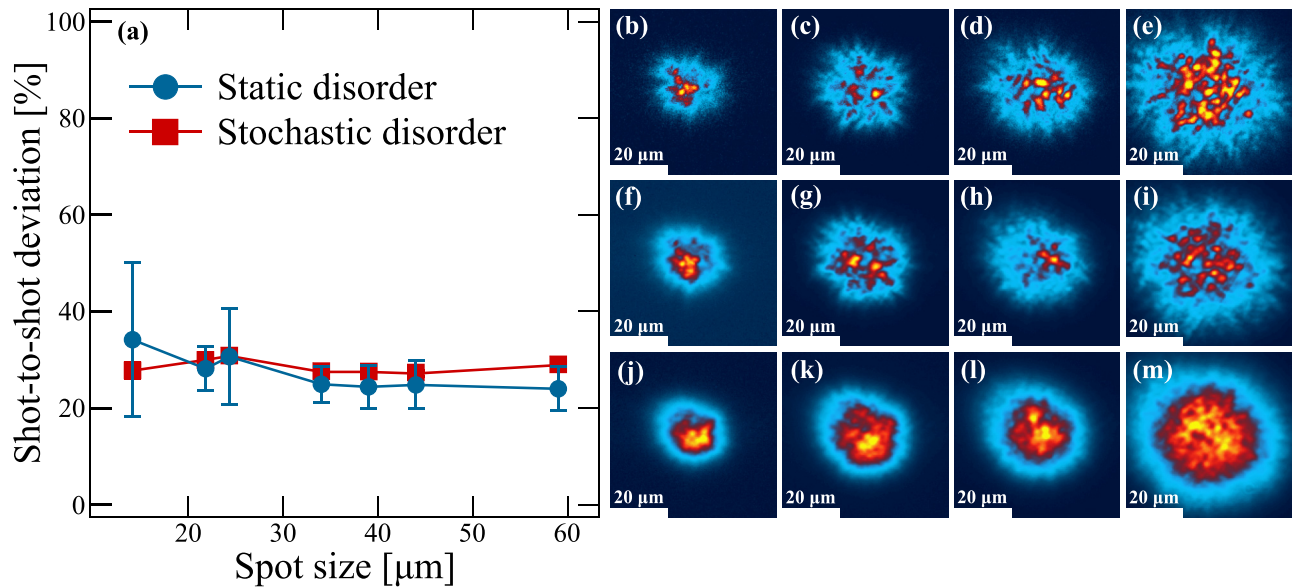


FIG. 6. (a) Dependence of static disorder, the divergence of a one-position time-averaged condensate profile from a many-position time-averaged condensate profile (blue circles), and stochastic disorder, the divergence of a single-shot condensate profile from a one-position time-averaged condensate profile (red squares), on the spot size. (b)–(e) Single-shot real-space profiles of a polariton condensate for four different spot sizes: 14, 22, 24, and 44 μm , respectively. (f)–(i) Corresponding one-position time-averaged real-space condensate profiles obtained from averaging 300 single-shot profiles over one position on the sample. (j)–(m) Corresponding many-position time-averaged real-space condensate profiles obtained from averaging one-position time-averaged real-space condensate profiles over eight different positions on the sample. Color scales are normalized to the maxima of these images.

in Fig. 6(a) to aggregate eight independent values and repeat the procedure for seven different spot sizes of the system.

Surprisingly, we do not observe any change in the static and stochastic contributions to the disorder with the change in the system size, which also does not correlate with the dependence of $g^{(2)}(0)$ on the system size in Fig. 4.

VI. CONCLUSION

To summarize, we studied the statistical, spectroscopic, and dynamic properties of organic polariton condensates at room temperature as a function of their size. We developed a technique for detecting single condensate realizations that provides access to photon statistics and allows one to study quantum statistical properties of room temperature light-matter condensates. Our findings demonstrate a high degree of coherence of the condensate with the second-order correlation function $g^{(2)}(0) = 1.00034 \pm 1 \times 10^{-5}$. For comparison, in high-contrast subwavelength gratings, $g^{(2)}(0) = 1.002 \pm 0.002$ was recorded [59], and in the cavity-integrated MoSe_2 monolayer, $g^{(2)}(0) = 1.004 \pm 0.003$ [65]; in both cases cryogenic temperatures were used. Our result of 100 times the shot noise obtained at room temperature is remarkable when one considers that in GaAs-based microcavities, noise of 50 times the shot noise was observed at cryogenic temperatures [49]. Single-shot imaging reveals the highly disordered nature of polariton condensates in both real and momentum space. We determined the static and stochastic contributions to the condensate disorder and demonstrated that the total shot-to-shot polariton number fluctuations are independent of the excitation spot size. Moreover, we showed the disorder

is independent of the system size, while the photon statistics get broader if we decrease the system size. We explained the behavior by the kinetic nature of polaritons, which starts to contribute to the losses once we enter the regime of small condensate sizes, inducing non-Poissonian intensity noise in the system. The interplay between kinetic polariton losses and thermalization defines the complex nonequilibrium dynamics of polariton condensates at room temperature, in sharp contrast to conventional laser behavior, leading to the discrepancy in the photon statistics. Besides fundamental aspects, this study indicates that room temperature polariton condensates comprise relatively low intensity noise despite their nonequilibrium and disordered nature. Given the recent advances achieved in polaritonics at room temperature [1,47,66,67], the noise performance demonstrated in this work appears to be very promising for all-optical signal processing enabling potential optical ultrafast switching at the fundamental energy level of a single photon in ambient conditions. It emphasizes the high application value of polariton devices with unique properties going far beyond the current state of the art and encourages further development of polariton coherent sources, amplifiers, switches, and logic gates.

ACKNOWLEDGMENTS

The authors sincerely thank D. Urbonas, T. Stöferle, and R. F. Mahrt for useful discussions and the provision of microcavity samples. A.D.P. and D.A.S. thank the support by the Russian Science Foundation (RSF), Grant No. 23-72-00059. E.S.A. and V.Yu.Sh. thank the Foundation for the Advancement of Theoretical Physics and Mathematics Basis.

- [1] A. V. Zasedatelev, A. V. Baranikov, D. Urbonas, F. Scafrimuto, U. Scherf, T. Stöferle, R. F. Mahrt, and P. G. Lagoudakis, A room-temperature organic polariton transistor, *Nat. Photonics* **13**, 378 (2019).
- [2] Y. Sun, P. Wen, Y. Yoon, G. Liu, M. Steger, L. N. Pfeiffer, K. West, D. W. Snoke, and K. A. Nelson, Bose-Einstein condensation of long-lifetime polaritons in thermal equilibrium, *Phys. Rev. Lett.* **118**, 016602 (2017).
- [3] A. Genco, A. Ridolfo, S. Savasta, S. Patanè, G. Gigli, and M. Mazzeo, Bright polariton coumarin-based OLEDs operating in the ultrastrong coupling regime, *Adv. Opt. Mater.* **6**, 1800364 (2018).
- [4] S. Shen, W. Yang, J. Shan, G. Sun, T.-M. Shih, Y. Zhou, and Z. Yang, Multiband enhanced second-harmonic generation via plasmon hybridization, *J. Chem. Phys.* **153**, 151102 (2020).
- [5] M. Dusel, S. Betzold, T. H. Harder, M. Emmerling, J. Beierlein, Jürgen Ohmer, Utz Fischer, R. Thomale, C. Schneider, S. Höfling, and S. Klembt, Room-temperature topological polariton laser in an organic lattice, *Nano Lett.* **21**, 6398 (2021).
- [6] S. Betzold, M. Dusel, O. Kyriienko, C. P. Dietrich, S. Klembt, J. Ohmer, U. Fischer, I. A. Shelykh, C. Schneider, and S. Höfling, Coherence and interaction in confined room-temperature polariton condensates with Frenkel excitons, *ACS Photonics* **7**, 384 (2020).
- [7] M. Dusel, S. Betzold, O. A. Egorov, S. Klembt, J. Ohmer, U. Fischer, S. Höfling, and C. Schneider, Room temperature organic exciton-polariton condensate in a lattice, *Nat. Commun.* **11**, 2863 (2020).
- [8] D. Sanvitto and S. Kéna-Cohen, The road towards polaritonic devices, *Nat. Mater.* **15**, 1061 (2016).
- [9] A. Graf, M. Held, Y. Zakharko, L. Tropsch, M. C. Gather, and J. Zaumseil, Electrical pumping and tuning of exciton-polaritons in carbon nanotube microcavities, *Nat. Mater.* **16**, 911 (2017).
- [10] A. Graf, L. Tropsch, Y. Zakharko, J. Zaumseil, and M. C. Gather, Near-infrared exciton-polaritons in strongly coupled single-walled carbon nanotube microcavities, *Nat. Commun.* **7**, 13078 (2016).
- [11] R. Su, A. Fieramosca, Q. Zhang, H. S. Nguyen, E. Deleporte, Z. Chen, D. Sanvitto, T. C. H. Liew, and Q. Xiong, Perovskite semiconductors for room-temperature exciton-polaritonic, *Nat. Mater.* **20**, 1315 (2021).
- [12] L. C. Flatten, Z. He, D. M. Coles, A. A. P. Trichet, A. W. Powell, R. A. Taylor, J. H. Warner, and J. M. Smith, Room-temperature exciton-polaritons with two-dimensional WS₂, *Sci. Rep.* **6**, 33134 (2016).
- [13] S. Dufferwiel, T. P. Lyons, D. D. Solnyshkov, A. A. P. Trichet, F. Withers, S. Schwarz, G. Malpuech, J. M. Smith, K. S. Novoselov, M. S. Skolnick, D. N. Krizhanovskii, and A. I. Tartakovskii, Valley-addressable polaritons in atomically thin semiconductors, *Nat. Photonics* **11**, 497 (2017).
- [14] L. K. van Vugt, S. Ruhle, P. Ravindran, H. C. Gerritsen, L. Kuipers, and D. Vanmaekelbergh, Exciton polaritons confined in a ZnO nanowire cavity, *Phys. Rev. Lett.* **97**, 147401 (2006).
- [15] G. Malpuech, A. Di Carlo, A. Kavokin, J. J. Baumberg, M. Zamfirescu, and P. Lugli, Room-temperature polariton lasers based on GaN microcavities, *Appl. Phys. Lett.* **81**, 412 (2002).
- [16] S. Kéna-Cohen and S. R. Forrest, Room-temperature polariton lasing in an organic single-crystal microcavity, *Nat. Photon.* **4**, 371 (2010).
- [17] J. D. Plumhof, T. Stöferle, L. Mai, U. Scherf, and R. F. Mahrt, Room-temperature Bose-Einstein condensation of cavity exciton-polaritons in a polymer, *Nat. Mater.* **13**, 247 (2014).
- [18] G. Lerario, A. Fieramosca, F. Barachati, D. Ballarini, K. S. Daskalakis, L. Dominici, M. De Giorgi, S. A. Maier, G. Gigli, S. Kéna-Cohen, and D. Sanvitto, Room-temperature superfluidity in a polariton condensate, *Nat. Phys.* **13**, 837 (2017).
- [19] F. Scafrimuto, D. Urbonas, M. A. Becker, U. Scherf, R. F. Mahrt, and T. Stöferle, Tunable exciton-polariton condensation in a two-dimensional Lieb lattice at room temperature, *Commun. Phys.* **4**, 39 (2021).
- [20] T. Yagafarov, D. Sannikov, A. Zasedatelev, K. Georgiou, A. Baranikov, O. Kyriienko, I. Shelykh, L. Gai, Z. Shen, D. Lidzey, and P. Lagoudakis, Mechanisms of blueshifts in organic polariton condensates, *Commun. Phys.* **3**, 18 (2020).
- [21] K. S. Daskalakis, S. A. Maier, and S. Kéna-Cohen, Spatial coherence and stability in a disordered organic polariton condensate, *Phys. Rev. Lett.* **115**, 035301 (2015).
- [22] N. Bobrovska, M. Matuszewski, K. S. Daskalakis, S. A. Maier, and S. Kéna-Cohen, Dynamical instability of a nonequilibrium exciton-polariton condensate, *ACS Photonics* **5**, 111 (2018).
- [23] K. S. Daskalakis, S. A. Maier, R. Murray, and S. Kéna-Cohen, Nonlinear interactions in an organic polariton condensate, *Nat. Mater.* **13**, 271 (2014).
- [24] T. Cookson, K. Georgiou, A. Zasedatelev, R. T. Grant, T. Virgili, M. Cavazzini, F. Galeotti, C. Clark, N. G. Berloff, D. G. Lidzey *et al.*, A yellow polariton condensate in a dye filled microcavity, *Adv. Opt. Mater.* **5**, 1700203 (2017).
- [25] M. Wei, S. K. Rajendran, H. Ohadi, L. Tropsch, M. C. Gather, G. A. Turnbull, and I. D. W. Samuel, Low-threshold polariton lasing in a highly disordered conjugated polymer, *Optica* **6**, 1124 (2019).
- [26] A. Öttl, S. Ritter, M. Köhl, and T. Esslinger, Correlations and counting statistics of an atom laser, *Phys. Rev. Lett.* **95**, 090404 (2005).
- [27] P. Schwendimann and A. Quattropani, Statistics of the polariton condensate, *Phys. Rev. B* **77**, 085317 (2008).
- [28] F. P. Laussy, G. Malpuech, A. Kavokin, and P. Bigenwald, Spontaneous coherence buildup in a polariton laser, *Phys. Rev. Lett.* **93**, 016402 (2004).
- [29] D. Sarchi and V. Savona, Spectrum and thermal fluctuations of a microcavity polariton Bose-Einstein condensate, *Phys. Rev. B* **77**, 045304 (2008).
- [30] M. Wouters and V. Savona, Stochastic classical field model for polariton condensates, *Phys. Rev. B* **79**, 165302 (2009).
- [31] J. Kasprzak, D. D. Solnyshkov, R. André, L. S. Dang, and G. Malpuech, Formation of an exciton polariton condensate: Thermodynamic versus kinetic regimes, *Phys. Rev. Lett.* **101**, 146404 (2008).
- [32] A. Askitopoulos, L. Pickup, S. Alyatkin, A. Zasedatelev, K. G. Lagoudakis, W. Langbein, and P. G. Lagoudakis, Giant increase of temporal coherence in optically trapped polariton condensate, [arXiv:1911.08981](https://arxiv.org/abs/1911.08981).
- [33] D. Sarchi and V. Savona, Long-range order in the Bose-Einstein condensation of polaritons, *Phys. Rev. B* **75**, 115326 (2007).
- [34] M. Pieczarka, E. Estrecho, M. Boozarjmehr, O. Bleu, M. Steger, K. West, L. N. Pfeiffer, D. W. Snoke, J. Levinsen, M. M. Parish *et al.*, Observation of quantum depletion in a non-equilibrium exciton-polariton condensate, *Nat. Commun.* **11**, 429 (2020).

- [35] S. Baryshev, A. Zasedatelev, H. Sigurdsson, I. Gnusov, J. D. Topfer, A. Askitopoulos, and P. G. Lagoudakis, Engineering photon statistics in a spinor polariton condensate, *Phys. Rev. Lett.* **128**, 087402 (2022).
- [36] A. H. Safavi-Naeini, J. Chan, J. T. Hill, S. Gröblacher, H. Miao, Y. Chen, M. Aspelmeyer, and O. Painter, Laser noise in cavity-optomechanical cooling and thermometry, *New J. Phys.* **15**, 035007 (2013).
- [37] C. M. Caves, Quantum-mechanical noise in an interferometer, *Phys. Rev. D* **23**, 1693 (1981).
- [38] C. Schneider, A. Rahimi-Iman, N. Y. Kim, J. Fischer, I. G. Savenko, M. Amthor, M. Lermer, A. Wolf, L. Worschech, V. D. Kulakovskii *et al.*, An electrically pumped polariton laser, *Nature (London)* **497**, 348 (2013).
- [39] N. G. Berloff, M. Silva, K. Kalinin, A. Askitopoulos, J. D. Töpfer, P. Cilibizzi, W. Langbein, and P. G. Lagoudakis, Realizing the classical XY Hamiltonian in polariton simulators, *Nat. Mater.* **16**, 1120 (2017).
- [40] S. Klembt, T. H. Harder, O. A. Egorov, K. Winkler, R. Ge, M. A. Bandres, M. Emmerling, L. Worschech, T. C. H. Liew, M. Segev, C. Schneider, and S. Höfling, Exciton-polariton topological insulator, *Nature (London)* **562**, 552 (2018).
- [41] A. Delteil, T. Fink, A. Schade, S. Höfling, C. Schneider, and A. İmamoğlu, Towards polariton blockade of confined exciton-polaritons, *Nat. Mater.* **18**, 219 (2019).
- [42] G. Muñoz-Matutano, A. Wood, M. Johnsson, X. Vidal, B. Q. Baragiola, A. Reinhard, A. Lemaître, J. Bloch, A. Amo, G. Noguees, B. Besga, M. Richard, and T. Volz, Emergence of quantum correlations from interacting fibre-cavity polaritons, *Nat. Mater.* **18**, 213 (2019).
- [43] J. D. Töpfer, H. Sigurdsson, L. Pickup, and P. G. Lagoudakis, Time-delay polaritonics, *Commun. Phys.* **3**, 2 (2020).
- [44] S. L. Harrison, H. Sigurdsson, S. Alyatkin, J. D. Töpfer, and P. G. Lagoudakis, Solving the max-3-cut problem with coherent networks, *Phys. Rev. Appl.* **17**, 024063 (2022).
- [45] D. Ballarini, A. Gianfrate, R. Panico, A. Opala, S. Ghosh, L. Dominici, V. Ardizzone, M. De Giorgi, G. Lerario, G. Gigli *et al.*, Polaritonic neuromorphic computing outperforms linear classifiers, *Nano Lett.* **20**, 3506 (2020).
- [46] R. Mirek, A. Opala, P. Comaron, M. Furman, M. Kr¹, K. Tyszka, B. Seredyński, D. Ballarini, D. Sanvitto, T. C. H. Liew *et al.*, Neuromorphic binarized polariton networks, *Nano Lett.* **21**, 3715 (2021).
- [47] A. V. Zasedatelev, A. V. Baranikov, D. Sannikov, D. Urbonas, F. Scafirimuto, V. Yu. Shishkov, E. S. Andrianov, Y. E. Lozovik, U. Scherf, T. Stöferle *et al.*, Single-photon nonlinearity at room temperature, *Nature (London)* **597**, 493 (2021).
- [48] V. Y. Shishkov, E. S. Andrianov, A. V. Zasedatelev, P. G. Lagoudakis, and Y. E. Lozovik, Exact analytical solution for the density matrix of a nonequilibrium polariton Bose-Einstein condensate, *Phys. Rev. Lett.* **128**, 065301 (2022).
- [49] A. P. D. Love, D. N. Krizhanovskii, D. M. Whittaker, R. Bouchekioua, D. Sanvitto, S. Al Rizeiqi, R. Bradley, M. S. Skolnick, P. R. Eastham, R. André, and L. S. Dang, Intrinsic decoherence mechanisms in the microcavity polariton condensate, *Phys. Rev. Lett.* **101**, 067404 (2008).
- [50] J. Wiersig, C. Gies, F. Jahnke, M. Aßmann, T. Berstermann, M. Bayer, C. Kistner, S. Reitzenstein, C. Schneider, S. Höfling *et al.*, Direct observation of correlations between individual photon emission events of a microcavity laser, *Nature (London)* **460**, 245 (2009).
- [51] M. Aßmann, F. Veit, M. Bayer, M. van der Poel, and J. M. Hvam, Higher-order photon bunching in a semiconductor microcavity, *Science* **325**, 297 (2009).
- [52] A. F. Adiyatullin, M. D. Anderson, P. V. Busi, H. Abbaspour, R. André, M. T. Portella-Oberli, and B. Deveaud, Temporally resolved second-order photon correlations of exciton-polariton Bose-Einstein condensate formation, *Appl. Phys. Lett.* **107**, 221107 (2015).
- [53] F. Scafirimuto, D. Urbonas, U. Scherf, R. F. Mahrt, and T. Stöferle, Room-temperature exciton-polariton condensation in a tunable zero-dimensional microcavity, *ACS Photonics* **5**, 85 (2018).
- [54] A. Perrin, R. Bücker, S. Manz, T. Betz, C. Koller, T. Plisson, T. Schumm, and J. Schmiedmayer, Hanbury Brown and Twiss correlations across the Bose-Einstein condensation threshold, *Nat. Phys.* **8**, 195 (2012).
- [55] E. Estrecho, T. Gao, N. Bobrovska, M. D. Fraser, M. Steger, L. Pfeiffer, K. West, T. C. H. Liew, M. Matuszewski, D. W. Snoke *et al.*, Single-shot condensation of exciton polaritons and the hole burning effect, *Nat. Commun.* **9**, 2944 (2018).
- [56] B. Schweitzer, G. Wegmann, D. Hertel, R. F. Mahrt, H. Bassler, F. Uckert, U. Scherf, and K. Mullen, Spontaneous and stimulated emission from a ladder-type conjugated polymer, *Phys. Rev. B* **59**, 4112 (1999).
- [57] P. R. Rice and H. J. Carmichael, Photon statistics of a cavity-QED laser: A comment on the laser-phase-transition analogy, *Phys. Rev. A* **50**, 4318 (1994).
- [58] See Supplemental Material at <http://link.aps.org/supplemental/10.1103/PhysRevB.110.045125> for the complementary experimental datasets and extended analysis, which includes Refs. [68–71].
- [59] S. Kim, B. Zhang, Z. Wang, J. Fischer, S. Brodbeck, M. Kamp, C. Schneider, S. Höfling, and H. Deng, Coherent polariton laser, *Phys. Rev. X* **6**, 011026 (2016).
- [60] C. Gardiner, P. Zoller, and P. Zoller, *Quantum Noise: A Handbook of Markovian and Non-Markovian Quantum Stochastic Methods with Applications to Quantum Optics*, Springer Series in Synergetics (Springer, Berlin, Heidelberg, 2004).
- [61] D. Porras and C. Tejedor, Linewidth of a polariton laser: Theoretical analysis of self-interaction effects, *Phys. Rev. B* **67**, 161310(R) (2003).
- [62] G. Nardin, K. G. Lagoudakis, M. Wouters, M. Richard, A. Baas, R. André, L. S. Dang, B. Pietka, and B. Deveaud-Plédran, Dynamics of long-range ordering in an exciton-polariton condensate, *Phys. Rev. Lett.* **103**, 256402 (2009).
- [63] D. W. Snoke and J. P. Wolfe, Population dynamics of a Bose gas near saturation, *Phys. Rev. B* **39**, 4030 (1989).
- [64] V. V. Belykh, N. N. Sibeldin, V. D. Kulakovskii, M. M. Glazov, M. A. Semina, C. Schneider, S. Höfling, M. Kamp, and A. Forchel, Coherence expansion and polariton condensate formation in a semiconductor microcavity, *Phys. Rev. Lett.* **110**, 137402 (2013).
- [65] H. Shan, J.-C. Drawer, M. Sun, C. Anton-Solanas, M. Esmann, K. Yumigeta, K. Watanabe, T. Taniguchi, S. Tongay, S. Höfling *et al.*, Second-order temporal coherence of polariton lasers

- based on an atomically thin crystal in a microcavity, *Phys. Rev. Lett.* **131**, 206901 (2023).
- [66] D. A. Sannikov, A. V. Baranikov, A. D. Putintsev, M. Misko, A. V. Zasedatelev, U. Scherf, and P. G. Lagoudakis, Room temperature, cascable, all-optical polariton universal gates, *Nat. Commun.* **15**, 5362 (2024).
- [67] D. Sannikov, T. Yagafarov, K. Georgiou, A. Zasedatelev, A. Baranikov, L. Gai, Z. Shen, D. Lidzey, and P. Lagoudakis, Room temperature broadband polariton lasing from a dye-filled microcavity, *Adv. Opt. Mater.* **7**, 1900163 (2019).
- [68] M. O. Scully and M. S. Zubairy, *Quantum Optics* (Cambridge University Press, Cambridge, 1997).
- [69] L. K. Thomsen, S. Mancini, and H. M. Wiseman, Continuous quantum nondemolition feedback and unconditional atomic spin squeezing, *J. Phys. B* **35**, 4937 (2002).
- [70] D. M. Whittaker and P. R. Eastham, Coherence properties of the microcavity polariton condensate, *Europhys. Lett.* **87**, 27002 (2009).
- [71] Y. Yamamoto and A. Imamoglu, *Mesoscopic Quantum Optics* (Wiley, New York, 1999).